Hybrid Wing-Body (HWB) Pressurized Fuselage Modeling, Analysis, and Design for Weight Reduction

Vivek Mukhopadhyay[1]
NASA Langley Research Center, Hampton, Virginia, 23681-2199

This paper describes the interim progress for an in-house study that is directed toward innovative structural analysis and design of next-generation advanced aircraft concepts, such as the Hybrid Wing-Body (HWB) and the Advanced Mobility Concept-X flight vehicles, for structural weight reduction and associated performance enhancement. Unlike the conventional, skin-stringer-frame construction for a cylindrical fuselage, the box-type pressurized fuselage panels in the HWB undergo significant deformation of the outer aerodynamic surfaces, which must be minimized without significant structural weight penalty. Simple beam and orthotropic plate theory is first considered for sizing, analytical verification, and possible equivalent-plate analysis with appropriate simplification. By designing advanced composite stiffened-shell configurations, significant weight reduction may be possible compared with the sandwich and ribbed-shell structural concepts that have been studied previously. The study involves independent analysis of the advanced composite structural concepts that are presently being developed by The Boeing Company for pressurized HWB flight vehicles. High-fidelity parametric finite-element models of test coupons, panels, and multibay fuselage sections, were developed for conducting design studies and identifying critical areas of potential failure. Interim results are discussed to assess the overall weight/strength advantages.

Nomenclature

a	=	rod-stringer or frame spacing (Fig. 2)
A	=	cross-sectional area of beam
A_{sx}	=	area of single longitudinal x-stiffener
A_{sy}	=	area of single transverse y-stiffener
b	=	frame or rod-stringer spacing measured along y axis
B	=	total breadth of stiffened panel between end supports
D	=	bending rigidity of plate $Et^3/12(1-\nu^2)$
D_x	=	bending rigidity of stiffened orthotropic plate about the y axis
D_y	=	bending rigidity of stiffened orthotropic plate about the x axis
E_x, E_y	=	Young's modulus of orthotropic plate in x and y directions
F_{cx}, F_{cy}	=	yield stress in compression along x and y directions
F_{tx}, F_{ty}	=	yield stress in tension along x and y directions
G	=	shear modulus
H	=	torsion stiffness of orthotropic plate
I	=	area moment of inertia for beam bending about neutral axis
I_x, I_y	=	area moment of inertia of x and y stiffeners about neutral axis
L	=	total length of stiffened panel or beam between end supports
ν_x, ν_y	=	Possion's ratio along x and y axis
N_x, N_y	=	running in-plane load along x and y directions
P	=	compression load on beam-column (Fig. 1)
P_{cr}	=	compression buckling load on beam-column
P	=	cabin pressure of 9.2 psi ($2P$ = 18.4 psi)
q	=	running normal load on beam
t	=	shell or skin thickness
w	=	beam or plate deflection
Z_{ox}, Z_{oy}	=	neutral axis location of x- and y-stiffeners from skin mid plane

[1] Senior Aerospace Engineer, Aeronautical Systems Analysis Branch, MS 442, AIAA Associate Fellow.

I. Introduction

Structural analysis and design of efficient pressurized fuselage configurations for first- and second-generation advanced aircraft concepts, such as the Hybrid Wing-Body (HWB) and Advanced Mobility Concept-X flight vehicles, has been a challenging problem for many years (Refs. 1-5). Compared with a conventional stiffened cylindrical fuselage, which is under hoop stress when pressurized, the box-type HWB fuselage is subjected to high bending stresses and deformations due primarily to the internal cabin pressure combined with in-plane compression loads. Under pressure loading, these bending stresses on flat panels are theoretically one order of magnitude higher than the (membrane) hoop stress in a conventional cylindrical fuselage of similar size and skin thickness. Moreover, the beam-column effect due to the axial compression from overall vehicle and wing bending can result in additional nonlinear stress and buckling. Hence, a significant structural weight penalty is incurred for the HWB class of vehicles when compared with a conventional Boeing 777 or Airbus A380 type of fuselage structure, unless the HWB pressurized fuselage structure is specially designed with bi-axially stiffened construction and lighter advanced composite materials. In addition, the resulting deformation of the aerodynamic surface could significantly affect the performance advantages that are provided by the large lifting body. Thus, an efficient fuselage structure configuration must be designed to reduce the overall deformation and weight penalty, while satisfying margins of safety and other failure criteria under the design-critical flight and ground loads.

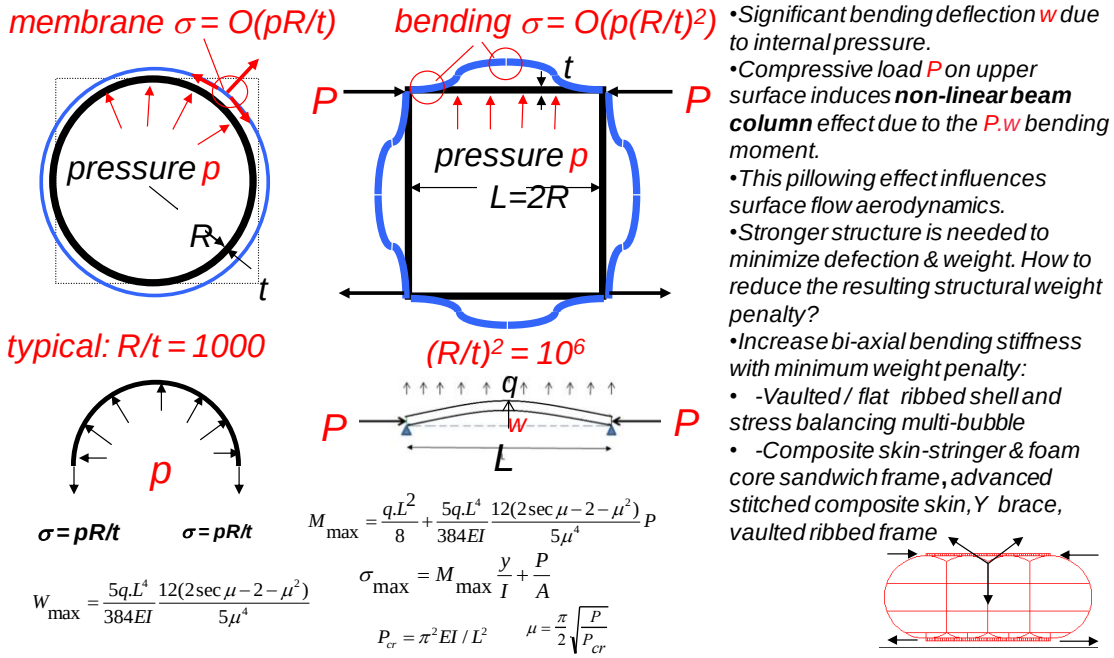

$$W_{\max} = \frac{5qL^4}{384EI}\frac{12(2\sec\mu - 2 - \mu^2)}{5\mu^4}$$

$$M_{\max} = \frac{qL^2}{8} + \frac{5qL^4}{384EI}\frac{12(2\sec\mu - 2 - \mu^2)}{5\mu^4}P$$

$$\sigma_{\max} = M_{\max}\frac{y}{I} + \frac{P}{A}$$

$$P_{cr} = \pi^2 EI / L^2 \qquad \mu = \frac{\pi}{2}\sqrt{\frac{P}{P_{cr}}}$$

Figure 1. Non-cylindrical pressurized-vehicle structural design challenges.

The design challenges that are associated with the design of an efficient non-cylindrical pressurized fuselage are outlined schematically in Fig. 1. When the cross section of a fuselage is circular, the internal pressure is resisted efficiently by the thin skin via hoop tension. The hoop stress, based on force equilibrium, is given by $\sigma = pR/t$, where p is the internal pressure, R is the fuselage radius, and t is the skin thickness. To maintain the shape under asymmetric bending loading and to prevent buckling, stiffening frames, stringers, and longirons are attached. The fuselage end pressure and the concentrated loads from the landing gear, engine, and wing mount are carried by heavy bulkheads, box beams and keel beams. On the HWB fuselage, the pressure load is balanced by bending stress instead of hoop stress. In addition, the compression on the upper fuselage surface due to the spanwise load creates additional stresses and deflections that are similar to those experienced for a

nonlinear beam-column design, as shown in Fig. 1. Non-linear beam-column equations and anisotropic plate theory (Refs. 6-10) are first briefly investigated to develop a tool for approximate parameter sizing and analytical prediction. The spread-sheet tool can also be utilized for analysis of bi-axially stiffened orthotropic plate and for possibly developing a semi-equivalent plate with similar structural characteristics under similar pressure loads.

Ideal beam-column analysis: A simple nonlinear beam-column analysis may provide some initial sizing information. Consider a cabin roof segment, as shown in Fig. 1, where P is the axial load, q is the distributed running load due to normal cabin pressure, and EI is the beam bending stiffness over the span- length L. The critical bucking load P_{cr} for a simple-supported boundary condition is given by $P_{cr} = \pi^2 EI/L^2$. From beam-column theory (Ref. 6), the maximum deflection, bending moment, and bending stress at mid-span are given by equations (1) through (3).

(1) $$w_{\max} = \frac{5q.L^4}{384EI}\frac{12(2\sec\mu - 2 - \mu^2)}{5\mu^4}$$

(2) $$M_{\max} = \frac{qL^2}{8} + \frac{5qL^4}{384EI}\frac{12(2\sec\mu - 2 - \mu^2)}{5\mu^4}P$$

(3) $$\sigma_{\max} = M_{\max}\frac{y}{2I} + \frac{P}{A}, \qquad \text{where } \mu = \frac{\pi}{2}\sqrt{\frac{P}{P_{cr}}}$$

For a simply supported beam with a transverse uniform distributed load *q/unit span*, the maximum linear deflection w is $5qL^4/384EI$ when the axial compression load P is zero. P_{cr} denotes the buckling load for axial compression. Note that the non-linear displacement w grows quite large as P is increased and approaches P_{cr}. Consider a beam length of L = 120 in. and a transverse running load of q = 9.2 pounds per inch. For a rectangular beam with a 2-in. height and unit width and $E = 9.25 \times 10^6$ pounds per square in. (psi), the maximum deflection is approximately 4 in. The buckling load P_{cr} is approximately 4,200 lb. With an axial compression load of 1,000 lb, the nonlinear deflection is 5.3 in. and the maximum compressive stress is 33,500 psi. Although equations (1) through (3) apply to a beam, they can be utilized for basic sizing and worst case study of a stiffened plate by replacing the beam bending stiffness EI/unit width with an equivalent stiffened plate bending stiffness, as follows.

Stiffened plate analysis: To achieve higher bending stiffness without increasing weight, deep sandwich and double-skin ribbed shell were studied in Refs. 4-5. In this paper, conventional stiffened shell and advanced stitched composite stiffened plates were studied by using linear plate theory and finite-element analysis. Consider the biaxially stiffened plate shown in Fig. 2. The equivalent bending stiffness D_x, D_y along the x and y directions and the torsional stiffness H of a biaxially stiffend plate of thickness t can be approximately defined by equations (4) through (6). Let us assume that the plate-theory assumptions are applicable to a stiffened plate. The frames, each with area A_{sx} and bending stiffness $E'_x I_x$ move the cross-sectional-area center by Z_{ox} from the plate neutral plane, thereby increasing the total area and the bending stiffness along the x axis. Similarly, the transverse stringers or rod-stiffeners, each with area A_{sy} and bending stiffness $E'_y I_y$, increase the bending stiffness D_y by moving the transverse-section-area center by Z_{oy} from the plate neutral plane. Based on the beam-column example, which has a cross-sectional area of 2 in^2 and an EI of 6.17×10^6 lb-in^2, the stiffener frame dimensions can be chosen to provide the section area and bending stifnesses of the same order.

(4) $$D_x = \frac{E_x t^3}{12(1-\upsilon_x\upsilon_y)} + \frac{E_x t Z_{ox}^{\ 2}}{12(1-\upsilon_x\upsilon_y)} + \frac{E'_x I_x}{b}$$

(5) $$D_y = \frac{E_y t^3}{12(1-\upsilon_x\upsilon_y)} + \frac{E_y t Z_{yo}^{\ 2}}{12(1-\upsilon_x\upsilon_y)} + \frac{E'_y I_y}{a}$$

(6) $$H = \frac{1}{2}(D_x\upsilon_y + D_y\upsilon_x + \frac{G_{xy}t^3}{3})$$

This fundamental sizing exercise can now be utilized to size a stiffening frame on a plate, as shown in Fig. 2. A foam-core frame with a height of 6 in. and a 4-in. flange with a 0.1-in. wrapped skin and a flange cover strap on a 0.5 in. thick core provide a skin cross-sectional area of approximately 2 in^2. The frame flange is stitched to the base skin and are spaced at b=20 in. interval. Then for a 0.1 in. skin thickness, the skin area between the frames is approximately 2 $in.^2$ Together, the skin segment and one frame will provide a running bending stiffness D_x of approximately 6.8×10^6 lb-in. Applying the simple-supported beam bending eqs. (1) through (3) with a 9.2-psi normal pressure load, the maximum deflection is 3.65 in. The critical beam-buckling load is 4,500 lbs, assuming that the unit acts like a simply-supported beam and the plate bending is neglected. With a compression load of 1,000 lbs, the nonlinear maximum deflection is 4.65 in., and the maximum bending stress on the frame top is approximately 85,000 psi without compression load. The maximum bending plus axial stress is approximately 90,000 psi with a 1000-lb compression load. In these beam bending calculations, *EI* is replaced with $D_x b$, and the total spanwise running load $q=9.2b$, where b is the frame spacing.

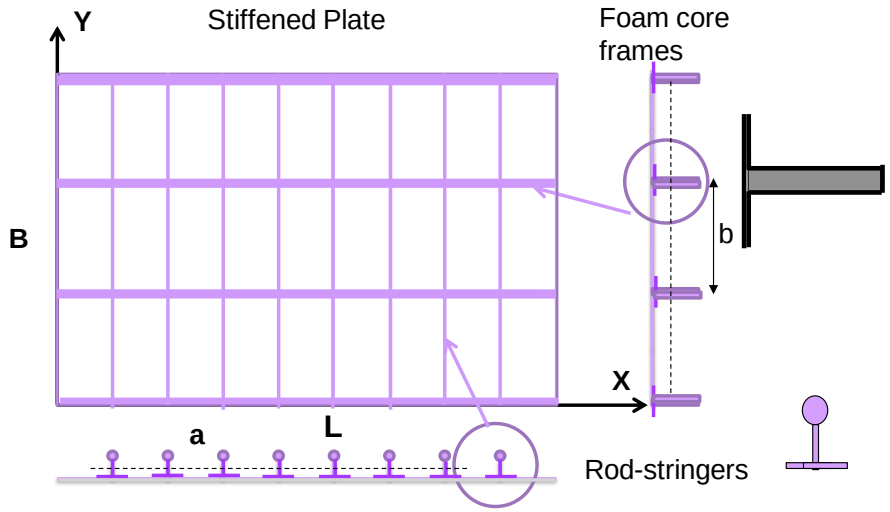

Figure 2. The orthotropic rod stringer and foam-core frame-stiffened plate.

Now let us apply these frame-stiffened plate stiffness estimates to the classical isotropic plate bending equations. The D_x that is computed for this frame-stiffened panel is now applied to a classical plate bending equation subject to a normal, uniform distributed pressure load of q psi with simple-supported and clamped-edge conditions. For a simply supported square plate, the maximum deflection is kqL^4/D with k = 0.00406 (Ref. 7, p. 197). For an anisotropic plate, if D is replaced by $sqrt(D_xD_y)$; then for q=18.4 psi, the maximum deflection for a 104-in. square panel is approximately 4.34 in. with $q=18.4$ psi, $D_x = 6.2 \times 10^6$ lb-in and $D_y = 0.65 \times 10^6$ lb-in.

For a square plate with built-in edges, the maximum deflection is kqL^4/D with k=0.00126 for B/L=1 (Ref. 7). If D is replaced by $sqrt(D_xD_y)$, then for a 104 in. square plate the maximum deflection is approximately 1.35 in. Alternatively, one can use anisotropic plate theory (Refs. 7–10) for a simply supported stiffened rectangular plate, for which the maximum deflection given by eq. (7).

$$(7)\quad w(x,y) = \frac{16q_o}{\pi^6} \sum_{m=1,3,5} \sum_{n=1,3,5} \frac{\sin(m\pi x/L)\sin(n\pi y/B)}{mn\left(\frac{m^4}{L^4}D_x + \frac{2m^2n^2}{L^2B^2}H + \frac{n^4}{B^4}D_y\right)}$$

If we apply the anisotropic plate data (q_o=18.4 psi, L=120 in., B=90 in., $D_x=8.4 \times 10^6$, $D_y=0.77 \times 10^6$) to this equation, then the maximum deflection of a simply-supported rectangular plate is computed to be approximately 5 in. with the frames running along the longer side, and 2.2 in. with the frames running along the shorter side (i.e., interchange D_x with D_y).

Conceptual structural analysis: Many structural concepts, such as conventional aluminum stiffened shells; stitched thick honeycomb-sandwich; ribbed double-shells; multi-bubble, vaulted shells; J-frame, beaded-hat stiffened shells; and advanced stitched, unitized, composite construction have been studied in-house and under both the Air Force Research Laboratory and National Aeronautics and Space Administration contracts (Refs. 11-21). Structural weight reduction with modern unitized construction has been a major effort and priority for both civilian and military aircraft (Refs. 12-13). In fact, structural weight reduction research and technology is a major component of the Environmentally Responsible Aviation (ERA) project at NASA. Further, a recent, highly promising innovation is the advanced pultruded-rod, stitched, efficient, unitized structure (PRSEUS) technology concept, which was developed at The Boeing Phantom Works for pressurized flight-worthy vehicles (Refs. 17-21). This paper describes interim progress and in-house independent study toward innovative structural concept analysis and design of the next generation HWB vehicles for structural weight reduction, that would lead to associated performance enhancement. The objective is to develop high-fidelity finite-element models (FEM) of test coupons, subcomponents, large panels, fuselage sections, and bulkheads, as well as of the full vehicle, and then conduct a parametric analysis to demonstrate the overall weight and strength advantages over other structural concepts that have been evaluated for the HWB concept. The progressive evolution of previous structural concepts is described next.

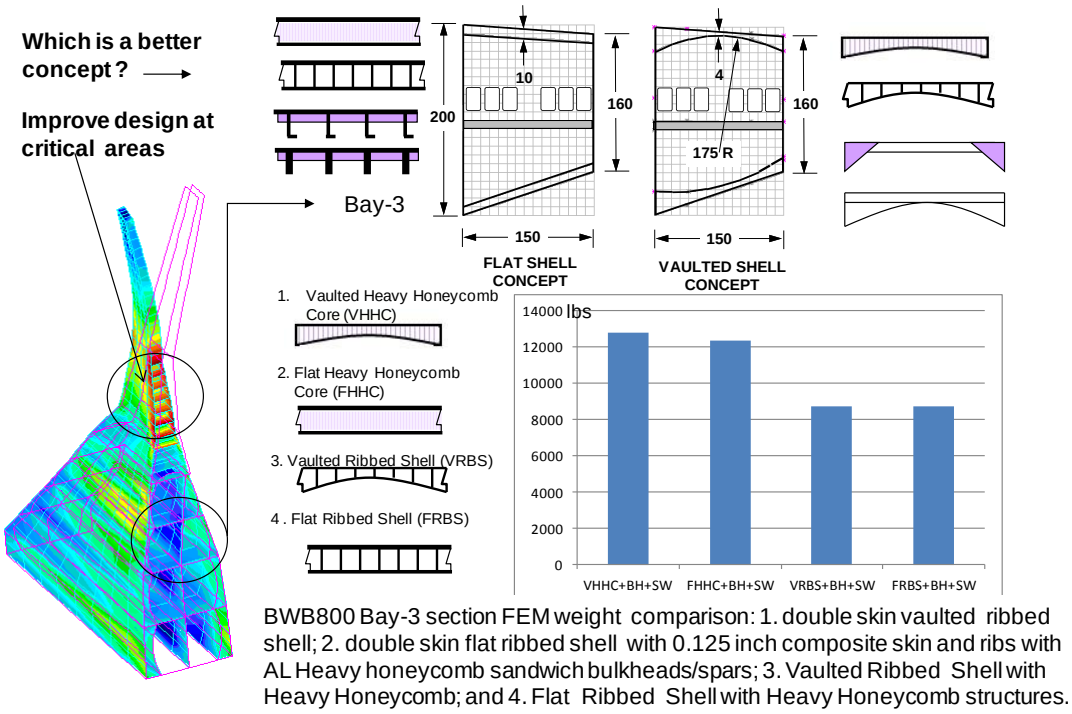

BWB800 Bay-3 section FEM weight comparison: 1. double skin vaulted ribbed shell; 2. double skin flat ribbed shell with 0.125 inch composite skin and ribs with AL Heavy honeycomb sandwich bulkheads/spars; 3. Vaulted Ribbed Shell with Heavy Honeycomb; and 4. Flat Ribbed Shell with Heavy Honeycomb structures.

Figure 3. Structural design trade study of an 800-passenger HWB vehicle and single bay with four concepts: (1) vaulted sandwich with heavy honeycomb core (VHHC); (2) flat sandwich with heavy honeycomb core (FHHC); (3) vaulted ribbed shell with double skin and heavy honeycomb sandwich spar/bulkhead (VRBS); and (4) flat ribbed shell with heavy honeycomb sandwich spar (FRBS).

The first- and second-generation 800-passenger HWB concepts were developed at Boeing Phantom Works both through independent internal research and under contract to NASA (Refs. 1–3). Additional conceptual fuselage designs were reported in Refs. 4 and 5. In Ref. 4, four structural concepts were studied, namely, (1) a vaulted sandwich with heavy honeycomb core (VHHC); (2) a flat sandwich with heavy honeycomb core (FHHC); (3) a vaulted, ribbed shell with double skin and heavy honeycomb sandwich spar, which also is a bulkhead (VRBS); and (4) a flat, ribbed shell with heavy honeycomb sandwich spar (FRBS). A structural design trade study of this 800-passenger HWB with these four concepts from Ref. 4 is summarized in Fig. 3. These studies were conducted with the following combined critical loading condition. The design ultimate cabin pressure differential at cruise condition was assumed to be 18.4 psi, which included all safety factors. The mid-deck passenger-floor loading was assumed to be 1 psi. The critical flight condition for limit load was assumed to be a 2.5-g maneuver at maximum takeoff weight. Typical bending moment, shear force, and

torque distribution based on elliptic spanwise loading on a swept cantilever beam were determined for the critical load case. These maneuver loads were multiplied by a safety factor of 1.5 to obtain the ultimate design loads.

Because both the vaulted sandwich shell concept and the flat sandwich shell concept are heavier, the double-skin flat or the vaulted, ribbed shell concept was preferable for weight reduction. If the FEM weights of these four concepts are divided by the component surface area of approximately 3,704 ft^2, which includes the top crown, passenger, and cargo floors, the side walls, and the front and rear spars (bulkheads), then the specific weigh per surface area can be used for comparison. This is shown in Fig. 4.

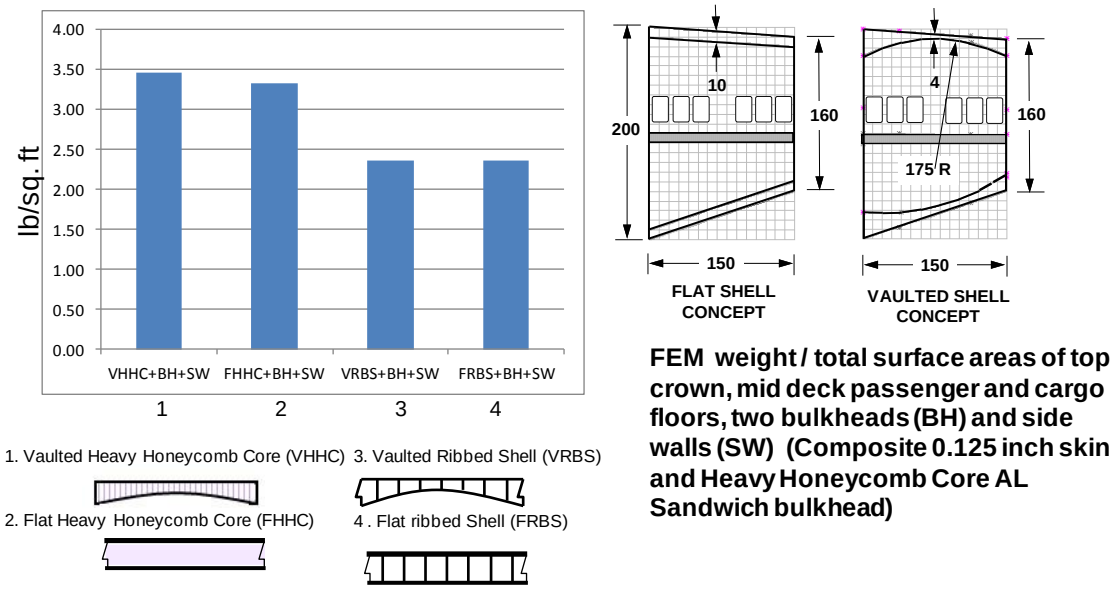

Figure 4. Specific FEM weight comparison for the third bay of an 800 passenger HWB concept.

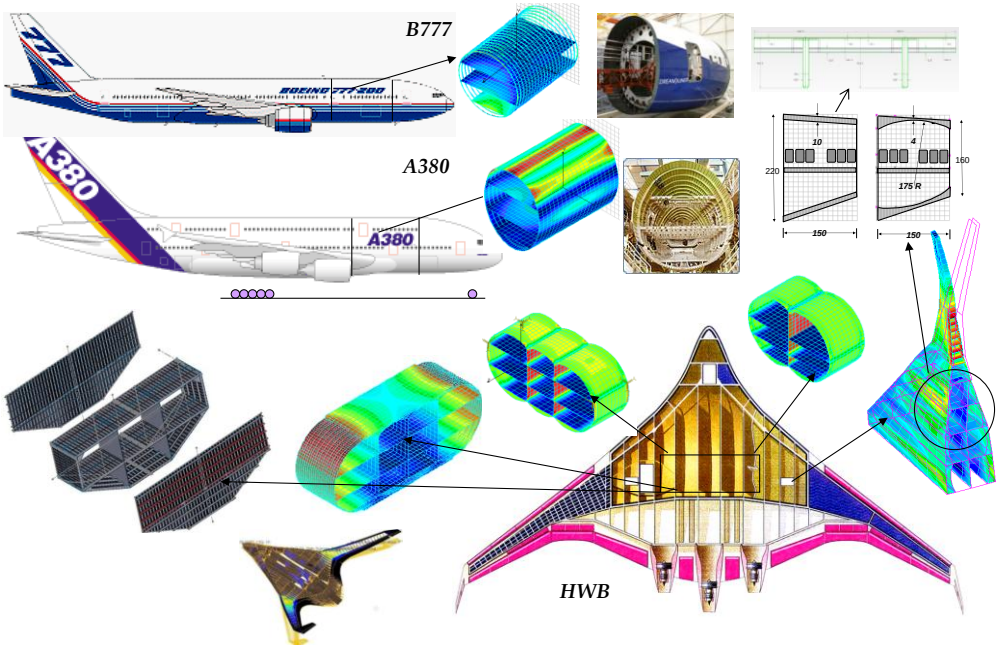

Figure 5. Fuselage section concept models of the B777, A380, and HWB class of vehicles.

Figure 5 shows a set of conventional and HWB structural concepts for a large transport aircraft fuselage that were used in both Ref. 5 and this paper for independent systems study and comparison. Although these studies considered widely different concepts, some of the specific weight results can be used for trend study. The initial results from these approximate finite-element analyses indicate progressively lower maximum stresses and deflections compared with the earlier study results that were reported in Ref. 4.

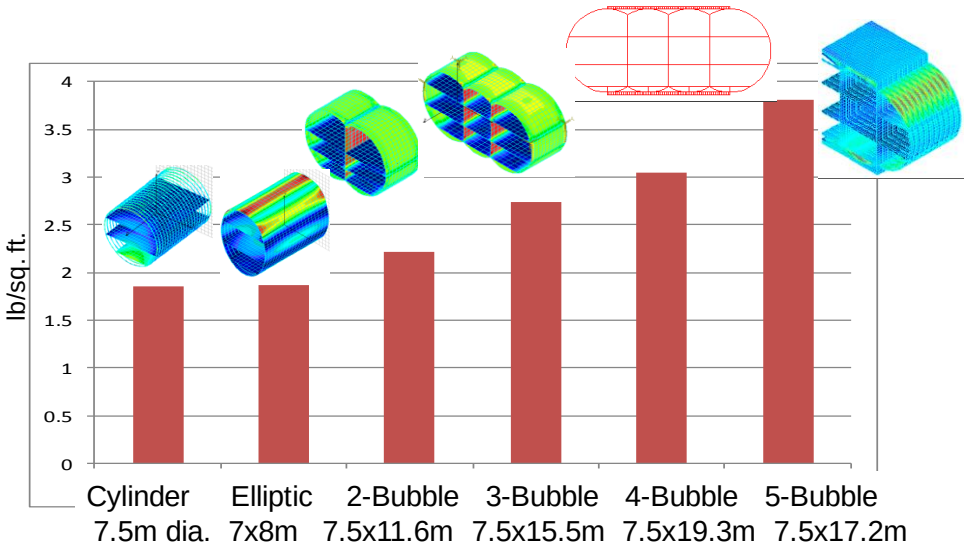

Figure 6. Relative conceptual FEM configuration weight per unit surface area.

Conventional two-floor cylindrical and A380-type elliptic sections and stress-balanced multi-bubble fuselage sections with frame- and stringer-stiffened aluminum skin were designed and analyzed with 18.4 psi pressure load. Each of these concepts had a 0.3-cm (0.118-in.) shell thickness and were stiffened with 10-cm high-I frames (Ref. 5). However, a relative comparison of the FEM weight per unit surface area of the segment unit, shown in Fig. 6, indicates that the unit weights/surface area of the multi-bubble concepts are relatively higher than those of the conventional cylindrical fuselage design. The surface area includes all outer shells and passenger floors. Although the stress-balanced multi-bubble design is very efficient, the increased weight is due to the redundant, double-skin design in the 4-bubble and 5-bubble cases. The inner skin can be eliminated by proper design of the frames and stringers for the critical load cases, combined with advanced stitched composite technology (Refs. 17-19) to increase the strength to weight ratio. Although, the FEM weight estimation comes from a conceptual structural design, the specific weight comparison shows the relative trend ranging from a surface area of 2 lb/ft^2 for the conventional fuselage section to nearly 4 lb/ft^{2}for the multi-bubble section. The double-skin flat or vaulted composite ribbed shell concepts shown in Fig. 4 can theoretically lower the range to 2.5 lb/ft^2. The present advanced stitched composite concept, which also addresses the damage tolerance and crack propagation concerns, can lead to additional weight advantage for both the conventional commercial aircraft and the HWB concept.

Aircraft composite structure: Modern commercial flight vehicles such as the B787 and the A380 have recently been built with advanced composite materials for both primary and secondary structure, which has resulted in significant weight reduction and performance enhancement. For example, compared to the all-aluminum B777, the new B787 aircraft has over 50 percent composite structure by weight. This has resulted in 20-percent greater fuel efficiency over that of the Airbus A330. The B787 also has a 60-percent smaller environmental noise footprint. In addition, for enhanced passenger comfort, the fuselage is designed for an operating cabin pressure of 12 psi, compared with the typical 9.2 psi in B777. Both the A380 structure and the B787 primary structure have demonstrated environmental and performance advantages due to the increased use of advanced composites.

Advanced stitched composite structure: The PRSEUS concept development may demonstrate that the HWB class of vehicles can be structurally as efficient as the conventional cylindrical skin-stringer-frame construction. For a detailed description of the PRSEUS concept, see Refs. 20 and 21. The basic stitched

composite skin is stiffened with pultruded rod-stringers and foam-core frames that run perpendicular to the rod stringers. The stitched resin-film–infused composite fabric wraps over the foam core. The frame flanges are also stitched to the skin and rod-frame junctions. This light-weight bi-axial stiffened construction provides significant bending rigidity. The stitching prevents crack propagation and inter-laminar separation. It also provides impact damage tolerance. In addition, the unitized construction reduces the part-count and the assembly time.

Unlike the conventional skin-stringer-frame construction for a cylindrical fuselage, the box-type pressurized PRSEUS panels in the HWB fuselage must be designed for minimal deformation of the outer surface. The structure must also have the required margins of safety for stress, strain, and buckling with a minimal structural weight penalty. These conflicting design requirements and constraints must be satisfied by considering a wide variety of design configurations, stiffener and frame spacing, and skin and frame wrap thicknesses in the weight optimization scheme. A set of high-fidelity FEMs is analyzed to arrive at a feasible design that meets these conflicting design objectives. A computer-aided design procedure was used to rapidly build parametric FEMs of the fuselage sections, wings, and full-vehicle structural assembly for conducting structural design studies (Refs. 22-25). For recent parametric design studies on the HWB vehicle aerodynamics, performance, and FEM based structural optimization and weight prediction, see Refs. 26-28. The iterative process of the FEM development and improvement is shown schematically in Fig. 7. A set of high-fidelity, hybrid FEMs was initially developed at the coupon, subcomponent, test-panel, fuselage-section, and bulkhead substructure levels for design and analysis. The pressure test-panel, fuselage section, and bulkhead models are improved via a set of design-scenario analyses. This paper discusses the significant results of this conceptual design study at each level.

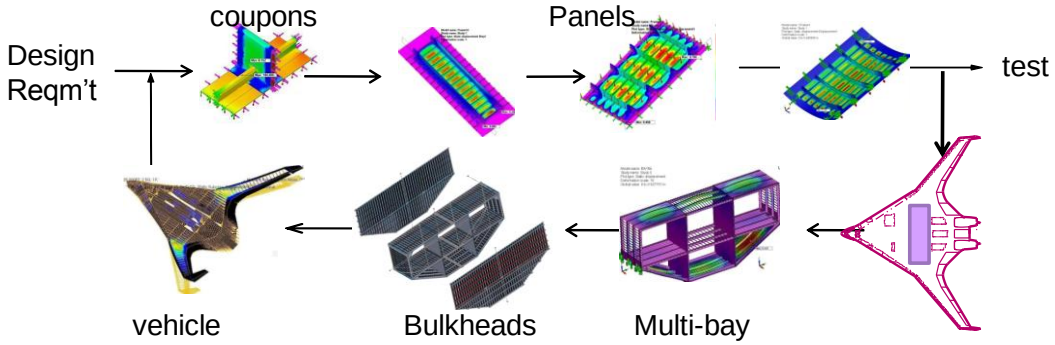

Figure 7. Schematic diagram of high-fidelity analysis and design process of advanced lightweight PRSEUS concept for a 200 passenger HWB vehicle structure and pressurized fuselage.

Design scenario analysis: The frame- and rod-stringer–stiffened plates were first studied analytically, as described earlier in this paper for sizing and to seek approximate solutions. Then, finite-element analyses were conducted with several suitable design scenarios with appropriate combinations of skin thickness, frame spacing, and rod spacing. The iterative analysis and design process steps were as follows:

- Develop baseline parametric Parasolid models to represent the PRSEUS concept at the coupon, subcomponent, panel, and fuselage section levels with appropriate levels of detail and idealization.
- Identify critical areas and improve FEMs at each level of detail. Compute stress, strain, deflection, weight, and safety margins with defined or estimated ultimate design loads and internal cabin pressures. Validate analysis with coupon and subcomponent test results.
- Determine stress, strain, deflection, and weight for a judicious combination of design scenarios with skin thickness (i.e., 0.05 and 0.1 in.), frame wrap thickness (i.e., 0.1 and 0.05 in.), rod-stringer spacing (i.e., 8 and 6 in.) and frame spacing (20 and 24 in.) for the pressurized components.
- Compare the results for an engineering optimization study for minimum weight while satisfying stress and strain constraints at critical locations. The following combinations of frame and rod spacing were selected for the stress reduction and weight optimization exercises: (1) frames with 20-in. spacing and rod stiffeners with 8-in. spacing; (2) frames with 24-in. spacing and rod stiffeners with 6-in. spacing. The rapid FEM analyses of several parametric configurations are documented to build a design database.

Design load conditions: The two critical load conditions are generally studied for the fuselage and bulkhead design: (1) a 2.5-g climb condition with an internal pressure of 9.3 psi (i.e., 1P-2.5g case) and (2) an 18.4-psi internal overpressure at ground level (i.e., 2P case). The maximum aerodynamic load for the 1P-2.5g case also produces a maximum compression load on the fuselage top panels and a maximum tensile load on the fuselage bottom panels. This bending load is idealized as approximately N_x=5,000-lb/in. running load along the top and bottom panels from full-vehicle FEM analysis results and includes all safety margins.

Material properties: The material properties are described in detail in Refs. 16 through 21. For the orthotropic stitched composite material, $E_x = 9.75 \times 10^6$ psi, $E_y = 4.86 \times 10^6$ psi, $\nu_x = 0.39$, $\nu_y = 0.2$, and the mass density is 0.057 lb/in^3. For the foam core, E = 21,000 psi, G = 7950 psi, and the mass density is 0.00361 lb/in^3. The web and the flange of the pultruded rod-stringer have the same property as the stitched composite material. The pultruded rod has an elastic modulus of E=1.9 × 10^7 psi and ν = 0.29. The stronger x-direction of the orthotropic skin and frame-wrap are always along the frame running direction.

Failure criteria: In the linear analysis, the maximum allowable principal strain of 0.007 was used for the orthotropic shell models of the skin and the frame wraps. For the orthotropic plate, average yield stress of F_y=46,500 psi was used for safety factor calculation. For the beam model of the built-up pultruded rod-stringer, F_y=46,500 psi, was also assumed. For solid models of the foam-core yield stress of F_y=440 psi was assumed. The allowable failure stresses of the orthotropic shell are F_{tx}=105,100 psi, F_{ty}=46,500 psi, F_{cx}=79,200 psi and F_{cy}=37,900 psi. The maximum allowable shear stress is 29,900 psi. When the rod stringers were modeled as beams, the maximum combined bending and axial stresses were used to check for beam failure. The directional stresses and principal strain distributions along with yield stress based factor of safety were plotted to identify local failure areas.

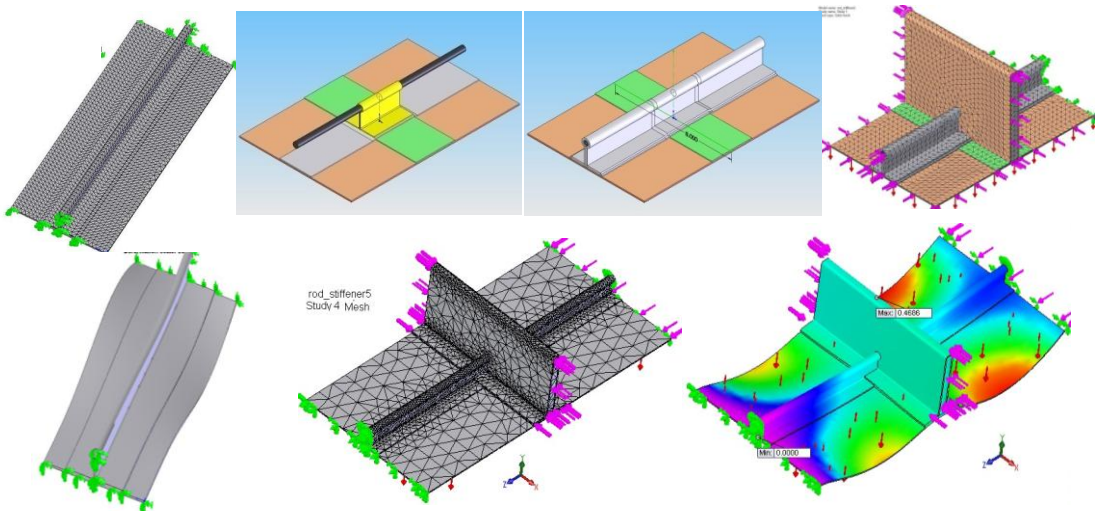

Figure 8. Baseline pultruded rod-stringer and frame-stiffened coupon model development.

Baseline coupon model: Because of the complex nature of the PRSEUS concept, understanding the structural characteristics of the pultruded rod-stiffener coupon and the rod-stringer–frame joint is important. These two subcomponents were studied first to identify the critical areas and to facilitate engineering approximations. An 18-in.-long, 6-in.-wide baseline rod-stringer–skin coupon with two-stack skin was analyzed for axial compression load and buckling study. The first four buckling end-loads were computed to be 23,000 lb, 25,000 lb, 28,000 lb, and 32,000 lb, respectively. These results were consistent with the buckling test data. Both this model and subsequent, simpler models were used to analyze stress and strain distributions, as well as buckling characteristics, to identify critical local failure areas. Figure 8 shows baseline pultruded rod-stiffener and foam-core-frame model development. These were first modeled with as-built solid elements and then approximated with a combination of rod, beam, solid, and shell elements. The most complex rod-stringer-frame model is used first to verify the test results and identify weak areas of local failure. Later, simpler, idealized models are used in bigger panels for rapid analysis and parametric study.

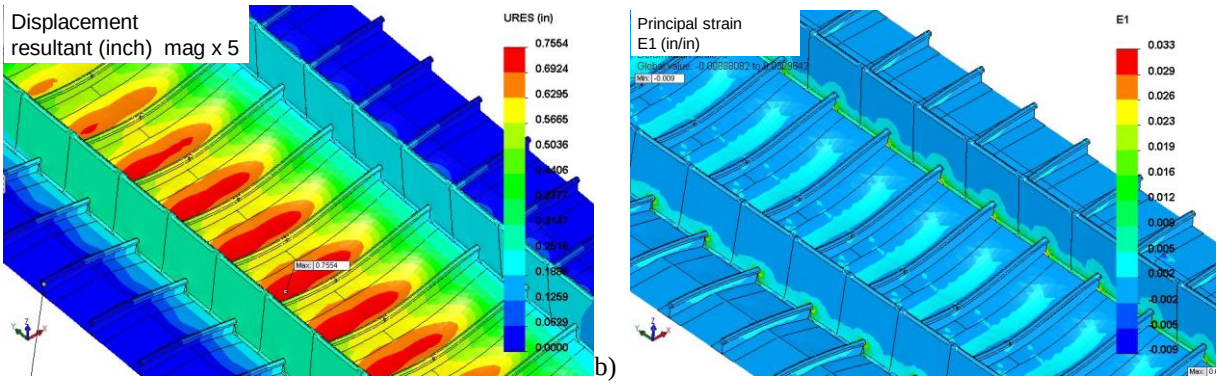

a) b)

Figure 9. FEM models of a 2-frame, 15-rod-stringer panel: (a) displacement and (b) principal strain with 18.4 psi pressure load.

Pressure test panel: Figure 9 shows a parametric PRSEUS panel in which the frame wrap, flange, frame-base strap, stringer web, flanges, and tear straps are modeled as shell elements. The pultruded-rod and wrap are merged and modeled with solid elements. The frame-core is modeled with solid elements and has keyhole cuts for rod-stringers to pass through. The initial model has 15 rod stiffeners spaced 6 in. apart and two frames spaced 20 in. apart. The rod stringers span the 40-in. width to the edge of the fixed side-edge splice. Figure 9(a) shows the deflection pattern for the case with a 0.052-in. (1-stack) skin and a 0.104-in. (2-stacks) frame-wrap with a normal pressure of 18.4 psi over the 90-in. by 30-in. area. The maximum deflection is 0.75 in. The frame-rod-stringer cut-through areas, top of rod-stringers and frame caps are critical high stress and strain areas, as can be seen in Fig. 9(b). In these areas, stress based factor of safety are locally below unity. This could lead to a slightly thicker skin and frame-top wrap design at a later stage for larger panels, where bending load is paramount. The single-stack skin/double-stack frame wrap and the double-stack skin/double-stack frame wrap combinations also were investigated for this panel and for a full fuselage section and bulkhead. Double-stack or thicker skins may be necessary for sections near the engine mount and other highly loaded sections where impact damage would be a concern. Also notice the large pillowing effect on the skin between the rod stringers. With a double-stack skin, this effect can be reduced by 50 percent or more. This periodic waviness would definitely affect the aerodynamics over the surface and could result in flow separation and turbulence. A similar test panel has been fabricated and tested with pressure and compression loads (refs. 29-30). These results were consistent with the pressure test data.

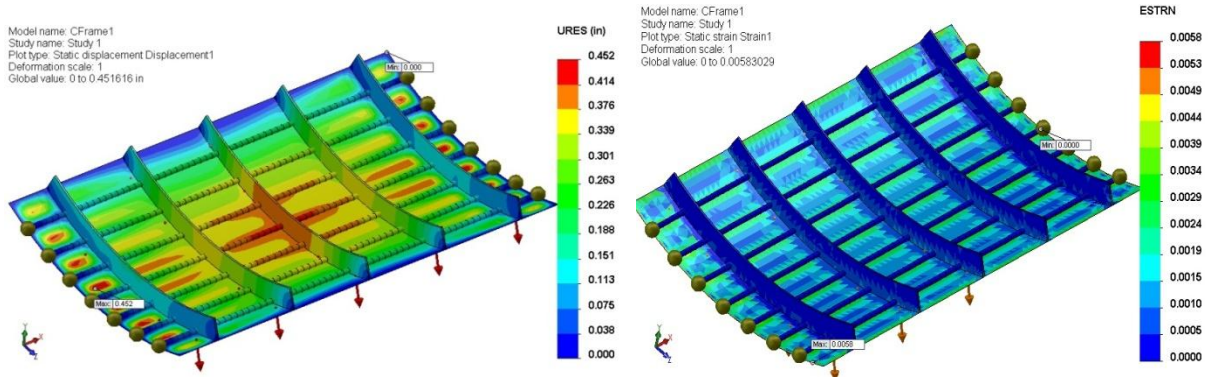

Figure 10. Curved PRSEUS panel model deflection, and equivalent strain with 18.4-psi pressure load and fixed-edge boundary condition.

Curved panel: Figure 10 shows the bending deformation and the equivalent strain on a curved panel with five frames with 20-in. spacing and seven rod stringers with 6-in. spacing. The analysis assumes a skin thickness of 0.052 in. (1 stack) and a 0.104-in. (2 stacks) frame wrap. Both the stresses and strains are generally within the allowable limits. The curvature allows the panel to contain the pressure by stretching and bending, while the rod stringers and frames help to maintain the cylindrical shape and prevent buckling. A similar curved PRSEUS panel is presently being fabricated and tested for pressure load and impact damage assessment (ref. 31).

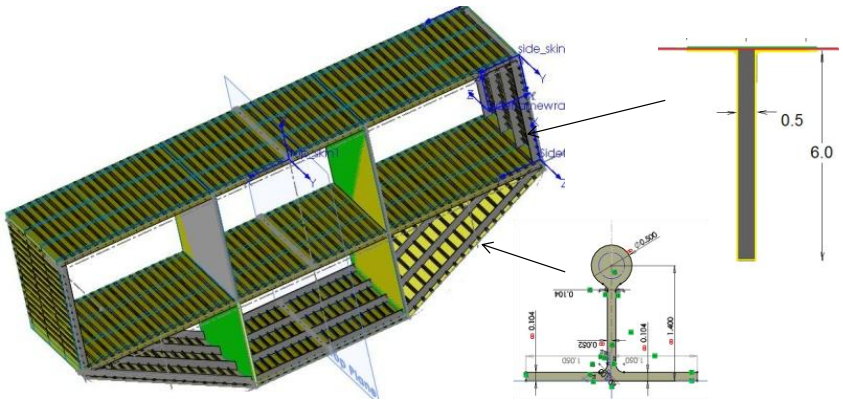

Figure 11. Multibay HWB fuselage section model (without end-pressure bulkheads) with four frames at 24-in. spacing, rod-stringers at 6 in. spacings on all outer walls and at 8 in. spacing on passenger floor.

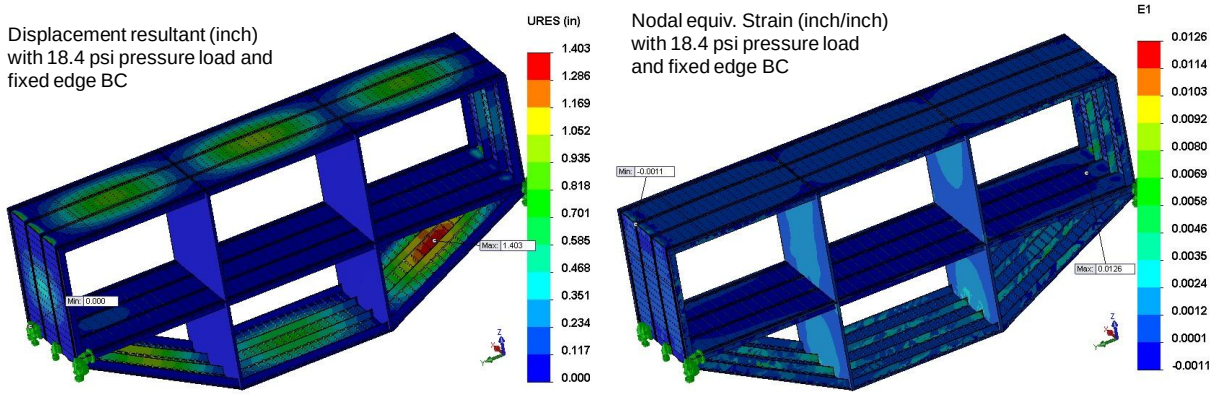

Figure 12. Four-frame multibay model displacement and element principal strain E1 under internal cabin pressure of 18.4 psi and passenger-floor pressure of 1 psi.

Multibay fuselage section: For a detailed description of the Multibay design, development, fabrication and combined loads test plan and progress, see Refs. 22, 32. Figure 11 shows a multibay concept model along with the frame and rod-stringer dimensions. This conceptual model is substantially simplified in features and dimensions from that described in refs. 22, 32 in order to study what-if type worst case scenario. This multibay is 360 in. wide in the spanwise direction with a height of 162 in. and a chordwise depth of 80 in. This fuselage section has four foam-core frames at 24 in. spacing. The 6 in. high, 0.5 in thick foam-cores are wrapped with 0.104 in. thick (2 stack) stitched composite wrap with 3.4 in. wide flanges and frame cover straps. The rod-stringers are spaced 6 in. apart on upper and lower surface of each bay, the side walls, and on the lower left and right cargo bay walls. The passenger floor rod-stringers are spaced at 8 in. apart. The rod-stringer flanges are 2 in. wide and the distance from the base to the rod-center is 1.4 in. These rod-stringers are modeled with beam elements. The two mid-cabin sandwich walls have 2 in. thick foam core and 0.052 in. stitched composite skin without cutouts. Figure 12 shows the displacements and principal strain E1 under 18.4 internal cabin pressure on all outer walls and 1 psi pressure on passenger floors. Since the bulkhead was not modeled, an all outer-edge-fixed boundary condition was applied. With all outer skin thickness of 0.052 in. (1 stack), the maximum deflection is about 1.4 in. at the center of lower cargo panel. The crown panel center-deflection is about 1.0 inch. The directional stresses and strains on the skin are generally within the allowable limits, except at edge-restraints, cabin-wall-skin junctions, corner junctions and foam-core frame areas. The maximum principal nodal strains are of the order 0.0126, at unreinforced cabin-corners and inter-cabin-junctions. In order to reduce large local stresses, these junctions need to be modeled more realistically with additional doublers or braces. These corner junction areas require diagonal braces and additional reinforcements, which were not modeled. Additional design refinements are required in these critical areas. The maximum bending and axial stresses on the rod-stiffeners, which were modeled as beam elements are generally within allowable limits, but may exceed locally at the lower cargo bay due to large bending. The stress safety factors on the rod-tops are locally below 1 and as low as 0.3 at the edge restraints and foam cores close to inter-cabin walls. These high

stresses can be mitigated by adding corner braces, rod-stiffeners with a higher bending stiffness and frames with thicker frame-caps in these areas along with at least 0.1 in. skin due to impact damage concerns.

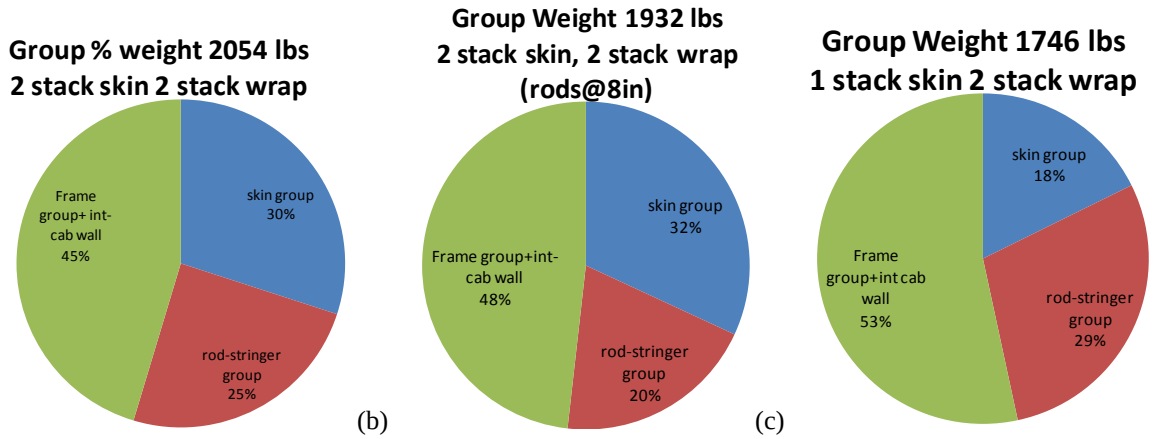

(a) (b) (c)

Figure 13. Group weight summary pie charts of multibay fuselage section for 3 design scenarios: (a) 2 stack skin, 2 stack wrap and rod spacing of 6 in.; (b) 2 stack skin, 2 stack wrap and rod-spacing of 8 in.; (c) 1 stack skin, 2 stack wrap and rod-spacing of 6 in. Passenger floor has 1 stack skin and rod-spacing of 8 in. in all 3 cases.

BAY4C New weight calculation with 1 stack skin and 2 stack wrap (80 inch width - 4 frame version)										
modified 24 in spacing 4 frames, 6 inch spacing rod with 1.4 base to rod center 2.1 flange, 3.4 in frame strap, 2 in int-cab core										
BAY6C new Sw11 2/12	width/seg	length	area	thickness	vol.	density	weight/each		weights	Group
	inch	in	in^2	in	in^3	lb/in^3	lbs	x no items	lbs	weight
skin group				1 stack skin						308
top panel	80	120	9600	0.052	499.2	0.057	28.5	3	85.4	
side panel	80	90	7200	0.052	374.4	0.057	21.3	2	42.7	
floor panels	80	120	9600	0.052	499.2	0.057	28.5	3	85.4	
bottom panels	80	120	9600	0.052	499.2	0.057	28.5	3.33	94.8	
modified rod 1.4 ht b2c	rod area	web area	flange are	area	length	density		no of rods		
rod-stringer group	in^2	in^2	in^2	in^2	in^3	lb/in^3	lbs	x no		506
rod_stringer	0.196349	0.108784	0.2184	0.523533	80	0.057	2.4	212	506.1	
modified frame wraps and straps				2 stack frame wrap						
Frame group+int cab wa	width	length	area	thickness	vol	110wf cSW		x no		932
frame core	6	120	720	0.5	360.0	0.0036	1.3	37.32	48.4	
frame wrap+flanges	15.9	120	1908	0.104	198.4	0.057	11.3	37.32	422.1	
inter cabin core	80	162	12960	2	25920.0	0.0036	93.3	2	186.6	
inter cabin wrap	80	162	12960	0.052	673.9	0.057	38.4	4	153.7	
side frame core	6	90	540	0.5	270.0	0.0036	1.0	8	7.8	
side core wrap+flange	15.9	90	1431	0.104	148.8	0.057	8.5	8	67.9	
frame cover strap	3.4	120	408	0.052	21.2	0.057	1.2	37.32	45.1	
max deflection 2P 1.4 in	0.5 inch with rod frame core and 1.4 inch with solid frame core						Total Weight (lbs)		1746	1746
Projected Surface area	with int-cab wall area		129911	in^2	902	sq feet			1.94	1746
	w/o int-cab wall area		103991	in^2		weight w/o 2 int-cab-wall			1.95	1406

Table 1. Weight calculation for case (c): 1 stack skin, 2 stack wrap and rod-spacing of 6 inches. Passenger floor has 1 stack skin and rod-spacing of 8 in. for all cases.

For the multibay parametric study, the weight analysis summary (without pressure bulkhead) pie charts showing the percentage contributions of the skin group, rod-stringer group and frame group are presented in Figure 13. Figure 13(a) shows the multibay group weight of 2054 lbs or 2.28 lbs/square feet with the surface area of 902 square feet including the mid-cabin walls. The maximum deflection is 1.3 in. in the cargo-bay area for this configuration with two stack skins and two stack frame-wrap and rod-stringer spacing of 6 inches. The weight can be reduced to 1932 lbs or 2.14 lbs/sq. feet by increasing the rod-stringer spacing from 6 in. to 8 in. on all outer walls (Fig. 3(b)). The maximum deflection in this case is of the order 1.7 in. at the lower cargo walls. The weight can also be reduced by using a single stack outer-skin configuration, but keeping the rod-stringer spacing at 6 in. on all outer walls. However with 1 stack skin, impact damage can be a concern. The estimated weight of the multibay for this case with

1 stack (0.052 in.) skin and 2 stack (0.104 in.) frame wrap (Figure 13(c)) is approximately 1746 lbs or about 1.94 lbs/square feet with the surface area of 902 square feet including the mid-cabin walls. Note that nearly 50% of the structural weight is contributed by the foam-core frame group and inter-cabin sandwich walls. The maximum deflection in this case is of the order 1.4 in. at cargo-bay center outer skin surface as shown in Figure 12. As noted earlier, rod-stiffeners with a higher bending stiffness and frames with thicker frame-caps will be required in this area. Table 1 shows detail of dimensions and weight calculation for the case (c) with 1 stack skin, 2 stack wrap and rod-spacing of 6 inches. Passenger floor has 1 stack skin and rod-spacing of 8 in. for all cases.

Conclusions

The knowledge of structural design techniques for nonconventional aerospace vehicles that is gained in this conceptual study provides designers with options for reducing the structural weights of pressurized, hybrid-wing-body (HWB) fuselages. An initial sizing study with classical beam-column and stiffened-plate analysis along with idealized finite element analysis of multibay section models indicate that advanced, stitched, composite stiffened plates with rod-stringers and foam-core frames are a viable alternative to double-skin-shell or multi-bubble construction. However, in order to reduce high local stress and pillowing effect farther in this design scenario study and to prevent buckling for combined cabin-pressure and compression load, as discussed in the beam-column sizing, rod-stiffeners with a higher bending stiffness and frames with thicker frame-caps will be required. Also, due to impact damage concern, the outer stiffened-skin thickness of at least 0.1 in. is preferable with marginal specific weight increase to about 2.3 lb/sq. ft, which is comparable to that of the cylindrical fuselage and better than multi-bubble concepts. This advanced, stitched composite technology could make the advanced HWB concept both structurally feasible and aerodynamically efficient. But, the adverse effect of pillowing on the HWB outer-surface aerodynamic flow should be considered. In addition to providing a technological advantage in the lucrative long-range travel market, the knowledge also could be applied to the design of highly pressurized conformal fuel tanks for reusable third-generation space exploration vehicles.

Acknowledgments

This research was done under the NASA Environmentally Responsible Aviation (ERA) and Subsonic Fixed Wing (SFW) projects in collaboration with both the Boeing Company, Huntington Beach, CA, and the Air Force Research Laboratory (AFRL). The author wishes to thank Dr. Fayette Collier, Project Manager, ERA Project; Anthony Washburn, Project Engineer; Dan Williams, Acting Head, Aeronautical Systems Analysis Branch, and William Kimmel, Acting Chief Technologist, Systems Analysis and Concepts Directorate; as well as the Fundamental Aeronautics Program office for funding this project. Test data, technical discussion and guidance from Alex Velicki and Dawn Jegley are greatly appreciated.

References

[1]Liebeck, R. H., "Configuration Control Document CCD-3: Blended Wing Body," Final report under contract NAS1-20275, NASA Langley Research Center, October 1997.

[2]Liebeck, R. H., Page, M. A., and Rawdon, B. K., "Blended-Wing-Body Subsonic Commercial Transport," AIAA-1998-0438, January 1998.

[3]Liebeck, R. H, "Design of the Blended Wing Body Subsonic Transport," *Journal of Aircraft*, Vol. 41, No. 1, Jan-Feb. 2004, pp. 10–25.

[4]Mukhopadhyay, V., "Structural Concepts Study of Non-circular Fuselage Configurations," AIAA/SAE WAC-67, World Aviation Congress, Los Angeles, CA, Oct. 22–24, 1996.

[5] Mukhopadhyay, V., Sobieszczanski-Sobieski, J., Kosaka, I., Quinn, G., and Vanderplaats, G., "Analysis, Design and Optimization of Non-cylindrical Fuselage for Blended-Wing-Body Vehicle," *Journal of Aircraft*, Vol. 41, No. 4, July-August, 2004, pp. 925–930.

[6]Timoshenko, S. P. and Gere, J. M., *Theory of Elastic Stability*, 2nd ed., Dover Publication, 2009, pp.1–45. Reprinted from McGraw Hill Book Co., New York, 1961.

[7]Timoshenko, S. P. and Krieger, S. W., *Theory of Plates and Shells*, 2nd ed., Dover Publication, 2009, pp.180–203, pp.365–377. Reprinted from McGraw Hill Book Co., New York, 1961.

[8] Paik, J. K., Thayamballi, A. K., and Kim, B. J., "Large Deflection Orthotropic Plate Approach to Develop Ultimate Strength Formulations for Stiffened Panels under Combined Biaxial Compression/Tension and Lateral Pressure," *Thin-Walled Structures*, Elsevier Publications (www.elsevier.com/locate/tws), Vol. 39, 2001, pp. 215–246.

[9] Hwang, I. and Lee, J. S., "Buckling of Orthotropic Plates under Various In-plane Loads," *KSCE Journal of Civil Engineering*, Vol. 10, No. 5, September 2006, pp. 349–356.

[10] Shimpi, R. P. and Patel, H. G., "A Two Variable Refined Plate Theory for Orthotropic Plate Analysis," *ASME Journal of Applied Mechanics*, Vol. 55, 2004, pp.7783–6799.
[11] Bradley, K. R., "A Sizing Methodology for the Conceptual Design of Blended-Wing-Body Transports," M.S. Thesis, Joint Institute for Advancement of Flight Sciences, George Washington University, Sept. 2004.
[12] Holzwarth, R. C., "The Structural Cost and Weight Reduction Potential of More Unitized Aircraft Structure," AIAA-1998-1872, April 1998.
[13] Hoffman, K., "Air Vehicle Technology Integration Program (AVTIP), Multi-role Bomber Structural Analysis," AFRL-VA-WP-TR-2006-3067, Final Report for 14 December 2004 – 08 May 2006, May 2006.
[14] Renton, J. W., Olcott, D., Roeseler B., Batzer, R., Baron, B., and Velicki, A., "Future of Flight Vehicle Structures," AIAA-2002-2023,, 2002. Also published in *AIAA Journal*, Vol. 41, No. 51, 2004, pp. 995–998.
[15] Velicki, A. and Hansen, D., "Novel Blended Wing Body Structures Concepts," BWB-NNL04AA36C-CLIN, The Boeing Company, Phantom Works, Final Report, Sept. 2004.
[16] Lovejoy, A. E, "Optimization of Blended Wing Body Composite Panels Using Both NASTRAN and Genetic Algorithm," NASA/CR-2006-214515, 2006.
[17] Velicki, A., Thrash, P. J., and Hawley, A. V., "Preliminary Design Requirements, Damage Arresting Composites for Shaped Vehicles," Mid-term Report, NASA Contract NNL07AA48C, December 2007 and April 2008.
[18] Velicki, A. and Thrash, P. J., "Advanced Structural Concept Development Using Stitched Composites," AIAA-2008-2329, 2008.
[19] Velicki, A., Thrash, P. J., and Jegley, D., "Airframe Development for the Hybrid Wing Body Aircraft," AIAA-2009-932, 2009.
[20] Velicki, A., "Damage Arresting Composites for Shaped Vehicles," Phase I Final Report, NASA/CR-2009-215932, Sept. 2009.
[21] Velicki, A., Yovanof, N., Baraja, J., Linton, K., Li, V., Hawley, A.,Thrash, P., DeCoux, S. and Pickell, R., "Damage Arresting Composites for Shaped Vehicles," Phase II Final Report, NASA/CR–2011-216880, January 2011.
[22] *Aerospace Design Engineer's Guide*, 5th Edition, AIAA Publications, Reston, Virginia, September 2003.
[23] Mukhopadhyay, V., Hsu, S-Y., Mason, B. H., Hicks, M. D., Jones, W. T., Sleight, D. W., Chu, J., Spangler, J. L., Kamhawi, H., and Dahl, J. L., "Adaptive Modeling, Engineering Analysis and Design of Advanced Aerospace Vehicles," AIAA-2006-2182, May 2006.
[24] *SolidWorks and SolidWorks Simulation User Manual 2011*, SolidWorks Corporation, Dassault Systèmes, Concord, Massachusetts, 2011.
[25] Mukhopadhyay, V., "A Conceptual Aerospace Vehicle Structural System Modeling, Analysis and Design Process," AIAA-2007-2372, April 2007.
[26] Gern, F., "Improved Aerodynamic Analysis for Hybrid Wing Body Conceptual Design Optimization, AIAA-2012-0249, 50th AIAA Aerospace Sciences Meeting, January, 2012.
[27] Nickol, C., "Hybrid Wing Body Configuration Scaling Study," AIAA-2012-0337, 50th AIAA Aerospace Sciences Meeting, January, 2012.
[28] Gern, F., "Finite Element Based HWB Centerbody Structural Optimization and Weight Prediction," AIAA Paper (TBP), 53rd AIAA/ASME/ASCE/AHS/ASC Structures, Structural Dynamics, and Materials Conference, April 2012.
[29] Lovejoy, A. E., Rouse, M., Linton, K. A., and Li, V. P., "Pressure Testing of a Minimum Gauge PRSEUS Panel," AIAA-2011-1813, 52nd AIAA/ASME/ASCE/AHS/ASC Structures, Structural Dynamics, and Materials Conference, Denver, April, 2011.
[30] Yovanof , N. P. and Jegley, D.C., "Compressive Behavior of Frame-Stiffened Composite Panels," AIAA-2011-1913, 52nd AIAA/ASME/ASCE/AHS/ASC Structures, Structural Dynamics, and Materials Conference, Denver, April 2011.
[31] Bergan, A., Bakuckas, J., Jr., Lovejoy, A., Jegley, D., Linton, K., Korkosz, G., Awerbuch, J., and Tan, T-M., "Full-Scale Test and Analysis of a PRSEUS Fuselage Panel to Assess Damage-Containment Features," 2011 Airworthiness & Sustainment Conference, San Diego, California, April 18-21, 2011.
[32] Velicki, A., and Jegley, D., "PRSEUS Development for Hybrid Wing Body Aircraft, "11th AIAA Aviation Technology, Integration and Operations Conference, AIAA Centennial of Naval Aviation Forum, Virginia Beach, Virginia, 2011.